Research Article | Vol. 27, No. 4 | 18 Feb 2019 | OPTICS EXPRESS 4238
Optics EXPRESS

Bichromatic pumping in mid-infrared microresonator frequency combs with higher-order dispersion

R. JOSEPH WEIBLEN,[1,2,*] AND IGOR VURGAFTMAN[1]

[1]Code 5613, Naval Research Laboratory, 4555 Overlook Ave. SW, Washington, DC 20375, USA
[2]ASEE Postdoctoral Fellow residing at NRL, Washington, DC, USA
[*]robert.weiblen.ctr@nrl.navy.mil

Abstract: Integrated microresonator-based mid-infrared frequency combs based on III-V semiconductors exhibit pronounced higher-order group velocity dispersion that can make it difficult to achieve stable output. One way to stabilize multiple solitons and their repetition rate is to pump simultaneously at two nearby comb lines. Two-color (or bichromatic) pumping also promises to boost the relatively low conversion efficiencies of single-soliton combs. We present simulations showing that, for a realistic InGaAs/InP ridge waveguide, the stabilization effect occurs over only a limited range of pump power and detuning parameters. We map out the parameter ranges for various regimes of operation in terms of the pump power and detuning and determine that the regimes converge quickly as the dispersion is truncated to progressively higher orders.

1. Introduction

Integrated mid-infrared (mid-IR) microresonator-based frequency combs show promise to revolutionize chemical sensing [1]. A novel and particularly interesting approach is to employ a moderate-gap III-V semiconductor as the microresonator material [2]. Since $\chi^{(3)} \propto E_g^{-4}$ [3], the nonlinearity is much higher than in state-of-the-art materials, which are wide-gap insulators and semiconductors. While silicon is a material system under intense study for microresonator combs [4], especially in the mid-IR, the direct gap of silicon (>3 eV), which governs its nonlinear effects, is much larger than its indirect gap, leading to a much smaller nonlinearity than in InGaAs. The material losses can be minimized by employing low-doped or semi-insulating semiconductors, and two-photon absorption can be nearly eliminated by tuning the energy gap E_g so that it is slightly higher than twice the maximum photon energy expected in the comb. For example, the InGaAs/InP material system is a good candidate for a comb centered on 4.5-5.0 μm, since the onset of two-photon absorption occurs at 3.3 μm. However, this approach makes it difficult to avoid pronounced higher-order group velocity dispersion (GVD) in ridge-waveguide-based resonators, which in turn complicates the attainment of stable broadband output. In particular, the repetition rate may become variable due to fluctuations in the pump power [5], and the observed comb output in a photodetector may be time dependent [6]. Such variability may be unacceptable if the combs are to find use in chemical sensing.

An interesting technique for stabilizing the repetition rate and multiple solitons is to pump simultaneously at two wavelengths separated by one or a few free spectral ranges (FSRs) of the microresonator. Previous theoretical work on bichromatic pumping [6-10] and modulated pumping [11,12] of microresonators has not included the effect of higher-order dispersion arising from the choice of materials, but it is precisely when such dispersion is present that the repetition rate of the frequency comb is difficult to fix, owing to the effect of the dispersion on the pulse velocity. In general, bichromatic pumping can employ two separate single-mode sources, or a specially designed dual-wavelength distributed-feedback emitter,

#346399 https://doi.org/10.1364/OE.27.004238
Journal © 2019 Received 26 Oct 2018; revised 7 Dec 2018; accepted 13 Dec 2018; published 5 Feb 2019

Optics EXPRESS

integrated on a single chip with the rest of the system. The results described in this work are applicable regardless of how the two pump wavelengths are generated. The presence of a second pump can also create a soliton crystal that remains stable for as long as the second pump is on. The nonlinear conversion efficiency then scales with the number of solitons in the crystal. The increase in the conversion efficiency afforded by soliton crystals is of great interest because the external nonlinear conversion efficiency in single-soliton systems is relatively low (~1%), being determined by the ratio of the pulse width and the round-trip time of the resonator [13]. This scheme for increasing the efficiency using bichromatic pumping is outlined in Section 4.

However, as we show below in Section 5, the range of relative pump strength, detuning, and loss needed for stabilization of the repetition rate is limited. These limitations have not been reported previously, even in systems with second-order dispersion (SOD) only. In this work, we also investigate the effect of changing the parameters of the pumps, including their relative frequency separation, relative power, total power, and the order of the group velocity dispersion of the microresonator, including second, third, sixth, and arbitrary orders. We show that dispersion terms beyond the second order can produce significant changes in the boundaries for the stable regions, and that the effect is due to a limited number of the higher-order terms.

The main results of this paper are found in Section 6, which presents the parameter ranges where the stabilization of the repetition rate by bichromatic pumping is effective for two different dispersion profiles. We also briefly compare these results to systems with SOD only in Section 7 and investigate the statistics of single-soliton comb generation using bichromatic pumping in Section 8.

2. Theoretical model

The simulations described here use a model based on the Lugiato-Lefever equation (LLE) [14,15]. The LLE with bichromatic pumping is given by:

$$t_R \frac{\partial E(t,\tau)}{\partial t} = \left[-\alpha - i\delta_0 + iL\sum_{k\geq 2} \frac{\beta_k}{k!}\left(i\frac{\partial}{\partial \tau}\right)^k + i\gamma L|E|^2 \right] E + \sqrt{\theta}\left(E_{\text{in}}^{(1)} + E_{\text{in}}^{(2)} e^{-i\varphi}\right) \quad (1)$$

where E is the field envelope, t is slow time (or lab time), τ is fast time, which follows the group velocity of the input field $E_{\text{in}}^{(j)} = \sqrt{P_{\text{in}}^{(j)}}$, where $P_{\text{in}}^{(j)} = P_j$ is the power of pump j, β_k are the terms in the GVD expansion around the center frequency, $\alpha = (\alpha_i + \theta)/2$ is the total round-trip amplitude loss due to absorption and coupling loss, α_i is the linear round-trip loss from material absorption, θ is the input power coupling factor, assumed to be the same for the two pumps with closely spaced wavelengths, L is the cavity length, t_R is the round-trip time, and δ_0 is the phase detuning of the pump with respect to the nearest cavity mode given by $\delta_0 = t_R(\omega_1 - \omega_p^{(1)})$, with ω_1 and $\omega_p^{(1)}$ being the frequency of the cavity resonance nearest the main pump and the main pump itself, respectively. The relative phase term φ accounts for a possible difference in detuning from the nearest cavity resonances that the two pumps might exhibit, i.e. $\varphi = t_R[(\omega_2 - \omega_p^{(2)}) - (\omega_1 - \omega_p^{(1)})]$. In Eq. (1), $\gamma = (2\pi n_2)/(\lambda A_{\text{eff}})$ is the Kerr nonlinear coefficient, $A_{\text{eff}} \approx 4.3\ \mu\text{m}^2$, calculated by COMSOL, is the effective modal area for the InGaAs/InP resonator specified below. We often use the normalized detuning parameter $\Delta = \delta_0/\alpha$ for the sake of generality. We also use $\delta_{ij} = t_R(f_i - f_j)$ to denote the frequency difference between the modes pumped by pump i and pump j, normalized to the FSR. When $\delta_{12} > 0$, the second pumped mode is on the short-wavelength (high-frequency) side of the main pump. In fact, the two pumps can have arbitrary frequency relative to the pumped modes, which is accounted for by δ_0, and the two pumps can have arbitrary frequency relative to each other, which is accounted for by φ, where φ is the detuning of the second pump from the nominal detuning.

Optics EXPRESS

Since n_2 in $In_{0.53}Ga_{0.47}As$ lattice matched to InP with E_g = 0.74 eV at room temperature is 2-3 × 10^{-12} cm^2/W using the material-independent constant and the strong dependence of the third-order nonlinearity on the energy gap derived in [3], we estimate $\gamma \approx 100$ $(W \cdot m)^{-1}$ for our resonator. However, the exact value γ of is not consequential, because stable combs can be found numerically for this system with γ = 10 $(W \cdot m)^{-1}$. In most calculations, we use the upper limit on the cavity loss of α_i = 0.0015 and $\theta = 1.1\alpha_i$, corresponding to a loaded Q ≈1 × 10^6 for an FSR of 100 GHz (for a total path length of 870 μm in the resonator) and a pump wavelength of λ_1 = 4.5 μm. The effect of higher losses is considered in Section 5.3. In these structures, two-photon absorption (2PA) is allowed only for λ < 3.35 μm, at the short-wavelength tail of the comb, and does not play a significant role in determining the loss. Three-photon absorption (3PA) is allowed for λ < 5 μm, but the peak 3PA is estimated to be negligible in the bus waveguide and in the resonator at the peak powers present in this system [16]. Since InGaAs layers can be grown with electron densities < 10^{15} cm^{-3} on semi-insulating InP substrates so that free-carrier absorption is very weak, in practice, the losses in such waveguides are likely to be limited by optical scattering from the roughness at the etched sidewalls.

Equation (1) is solved using a symmetrized split-step Fourier transform method, in the same manner as for supercontinuum generation [17]. We use 2^{13} time/frequency points and a slow-time step size of $t_R/30$. We have verified that increasing the discretization in either dimension does not change the results of the simulations. To handle the inhomogeneous forcing term, we include it with the linear part of the equation, and apply variation of parameters and a second-order Rosenbrock-Euler exponential integrator [18].

Practically, since the forcing term is grouped with the linear part of the equation, and the linear part is solved in the Fourier domain, we include the second pump by first taking the transform of the main pump term and adding the second pump to the appropriate frequency in the Fourier domain. This yields a time-domain picture of the pump with a standing wave-like interference pattern. The two pumps can then simply be detuned simultaneously, or at different rates by separately changing the detuning of the second pump in the frequency domain.

In this work, we present results for a 3 μm wide × 2 μm tall rectangular cross-section InGaAs/InP resonator, as shown in the inset to Fig. 1(a), with a 100 GHz free spectral range (FSR) and the exact GVD calculated by COMSOL, using the wave-optics module. The calculated dispersion for this geometry represents the widest spectral width between the zero-dispersion wavelengths of all the simulated resonators with a rectangular cross section. We also present results for resonators characterized by various truncations of the eighth-order Taylor series approximation (from β_2 to β_{10}) to the exact calculated dispersion, given in Table 1. Also given in Table 1 are the normalized dispersion coefficients, defined by $d_k = (2\alpha/|\beta_k|L)^{k/2}\beta_k L/(\alpha k!)$ [19]. Figure 1(a) shows dispersion curves for the exact GVD and the truncations used in this work as $\beta_2(\omega) = \sum_{k=2}^{n} \beta_k (\omega - \omega_0)^k / k! = \beta(\omega) - \beta(\omega_0) - \beta_1(\omega_0)$, where ω_0 is the angular frequency of the pump and n is the maximum dispersion order.

Table 1. Dispersion Coefficients

Coefficient	Value	Unit	Normalized Value
β_2	−1000.7	ps^2/km	−1
β_3	35.1	ps^3/km	0.0650
β_4	1.13856	ps^4/km	0.0039
β_5	−0.1084	ps^5/km	-6.89×10^{-4}
β_6	0.00309	ps^6/km	3.63×10^{-5}
β_7	1.02×10^{-4}	ps^7/km	2.22×10^{-6}
β_8	-8.745×10^{-6}	ps^8/km	-3.51×10^{-7}
β_9	1.02×10^{-7}	ps^9/km	7.59×10^{-9}
β_{10}	7.089×10^{-9}	ps^{10}/km	9.76×10^{-10}

Optics EXPRESS

We have verified that the results in this work are not sensitive to the exact detuning of the two pumps. The results should also be qualitatively applicable to other material systems with moderate energy gaps. Similar results are obtained for different power levels, as long as the detuning is adjusted accordingly. Unless otherwise noted, we consider a main pump with power P_1 = 5 mW at 4.5 μm, without loss of generality, since in the modeling, the central frequency drops out of the computational scheme. We also take $P_2 \leq P_1$, without loss of generality.

Whereas the simulation results in this work primarily use soliton initial conditions, similar results can be obtained by starting from noise and gradually increasing the detuning, as in the conventional experimental technique for generating a microresonator comb. However, the use of soliton initial conditions considerably reduces the computation time and increases the efficiency (by eliminating the cases with no solitons at the conclusion of the simulation run). The statistics of soliton generation in these resonators from white-noise initial conditions are discussed further in Section 8.

3. Bichromatic pumping scheme

If the second pump is not present and a resonator exhibits third-order dispersion (TOD) or higher, the repetition rate may fluctuate owing to small variations in the pump power and other parameters. Since the group velocity β_1^{-1} has been removed from the model by a change of variables, a pulse with a pump-power-dependent repetition rate will appear in the simulations to rotate around the resonator represented by the periodic simulation window of the fast-time span, i.e., the velocity of the pulse peak is different from the nominal group velocity [20], with the exact value that depends on the pump power. Figure 1(b) shows the typical result with a constant rotation speed when all orders of dispersion (AOD) is present, meaning that the dispersion is exactly as calculated in an approximation free manner using $\beta_2(\omega) = \beta(\omega) - \beta(\omega_0) - \beta_1(\omega_0)$. Figure 1 shows that a single soliton pulse is generated in the resonator within the 10 ps round-trip time of the resonator evolving over the slow-time axis for more than 200 ns. The pulse moves from right to left across the periodic simulation window, with the direction and velocity determined by the sign and the magnitude of the TOD, respectively. Because the TOD leads to an increase in soliton velocity over the group velocity, a dispersive wave (also known as optical Cherenkov radiation) is generated at a wavelength that is phase matched to the pump.

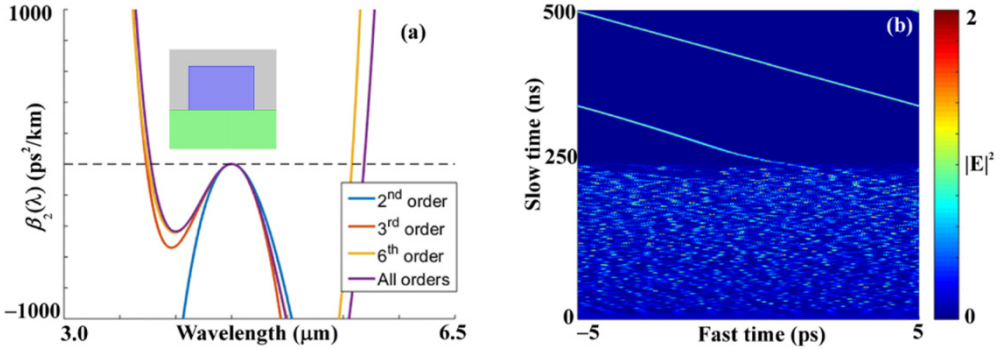

Fig. 1. (a) Dispersion curves for SOD (blue), TOD (orange), sixth-order dispersion (6OD) (yellow), and AOD (violet). The inset (a) shows the resonator cross-section, with InP substrate (green), 3 μm wide x 2 μm tall InGaAs core (blue), in air (gray). The quantity $\beta_2(\omega)$ is defined in the text. On the short-wavelength side, the curves for TOD, 6OD, and AOD overlap so closely that they are nearly indistinguishable. (b) A single soliton, generated from noise by increasing the detuning from Δ = 0 to Δ = 31.5, rotating in a system with monochromatic pumping and AOD.

Optics EXPRESS

Figure 2(a) shows a system with AOD and bichromatic pumping. The second pump is one FSR above the main pump frequency ($\delta_{12} = 1$) and has $P_2 = 3$ mW ($P_2/P_1 = 60\%$). In this case, a single soliton results from the random initial conditions as the detuning is increased, as in the conventional approach for generating soliton combs. Soon after being generated, this soliton moves left, as in Fig. 1(b), but quickly comes to a stop at a position just to the left of the mid-point of the resonator. This point is near a minimum in the intracavity input pump power determined by the interference of the two pumps. The effect of the minimum of the intrcavity pump wave is visible in Fig. 2(a) by the reduced amplitude of radiation near zero in fast time. The pulse position is stable in this location for the balance of the simulation, so the repetition rate remains fixed without any electronic locking (provided the pump frequencies remain stable with respect to each other). In the following, "stability" refers to the reduced impact of the pump intensity noise on the repetition rate rather than to the existence of the soliton or the invariance of the comb envelope. Figure 2(b) shows the spectrum corresponding to the stable solution in Fig. 2(a) and similar spectra for 6OD and TOD, all with $\delta_{12} = 1$ and $P_2/P_1 = 60\%$. The differences in the spectral locations of the dispersive wave peaks correspond to the zeros of β_2 seen in Fig. 1(a) [5].

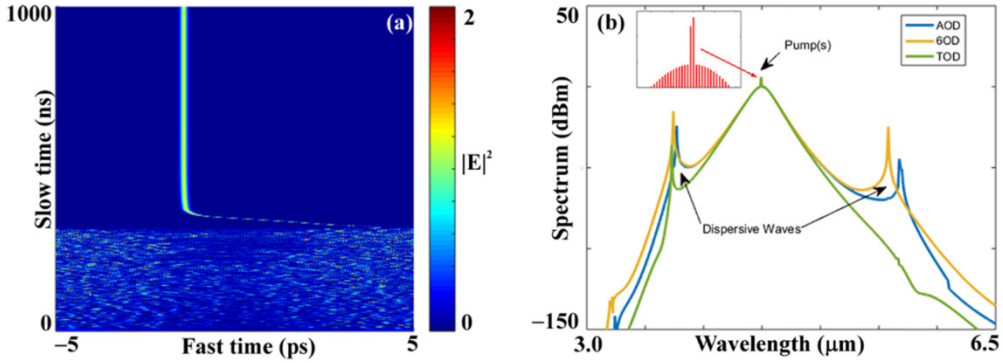

Fig. 2. (a) A single soliton, generated from noise by increasing the detuning by increasing the detuning from $\Delta = 0$ to $\Delta = 31.5$, at a fixed position in the simulation of a system with bichromatic pumping and AOD. (b) Spectra corresponding to a single, stabilized soliton in a system with $\delta_{12} = 1$ and $P_2/P_1 = 60\%$ and AOD (blue), 6OD (yellow), and TOD (green).). The inset shows a close-up of the pump region, showing two pumps at adjacent resonator modes with $P_2/P_1 = 60\%$ and $\delta_{12} = 1$.

To elucidate the mechanism of stabilization, we show in Fig. 3(a) a soliton in a system with TOD. We neglect higher orders of dispersion because higher-order terms do not significantly affect the stabilization dynamics related to bichromatic pumping. Nevertheless, they may significantly affect the comb spectrum, possibly by the introduction of additional dispersive waves as shown in Fig. 2(b), and the statistics of soliton generation, making it less likely that one or more solitons emerges from noise. However, the parameter range for effective stabilization is approximately the same as for higher-order dispersion, as shown in Section 6. In the simulation shown in Fig. 3(a), the pump is initially monochromatic, but a second pump with $\delta_{12} = 1$ and $P_2/P_1 = 60\%$ is turned on at 250 ns and off at 500 ns, both of the events being instantaneous. Figure 3(b) shows the calculated momentum of the intracavity field depicted in Fig. 3(a) as a function of slow time, defined as [21]:

$$P = \frac{1}{2}\int_{-t_R/2}^{t_R/2} d\tau E^* \left(-i\frac{\partial}{\partial\tau}\right) E + \text{c.c.} \qquad (2)$$

where E is the intracavity field envelope, as before. Under monochromatic pumping, the momentum quickly decays to zero, indicating that no effective force is acting on the pulse in steady state. This is consistent with previous results [21], which found solutions with zero

Optics EXPRESS

momentum, but nonzero velocity. When the second pump is turned on, the momentum executes one oscillation and then settles on a non-zero value as the pulse position stabilizes. Here the "force" applied by the interference pattern of the pumps counteracts the drift of the pulse due to the higher-order GVD. When the second pump is turned off again at 500 ns, the momentum quickly decays to zero, and the pulse recommences its rotation in the simulation window.

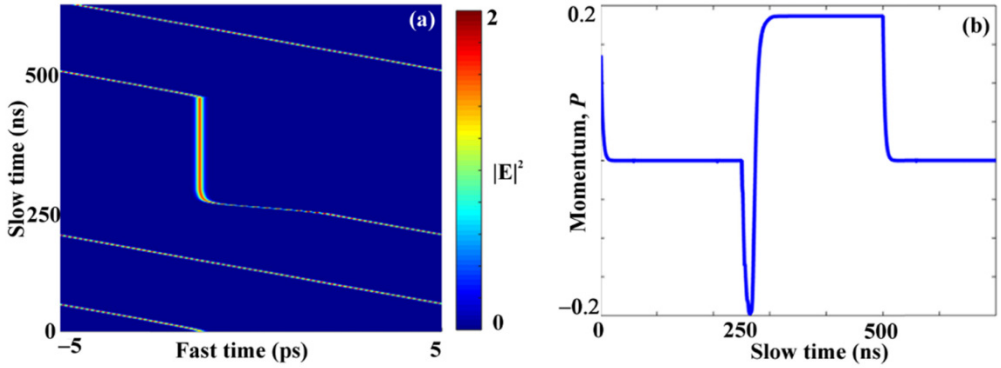

Fig. 3. (a) A single pulse in a resonator at Δ = 31.5 with the second pump turned on at 250 ns and off again at 500 ns. (b) The calculated momentum for the evolution shown in (a).

4. Efficiency increase

Since pulses preferentially rest at resonator positions near the pump interference minimum, multiple stable pulses in a resonator can be obtained by increasing the separation between the two pumps to higher multiples of the FSR, as shown schematically in Fig. 4(a). This allows the efficiency of a soliton comb to scale with the number of solitons, which are evenly spaced throughout the resonator because of the equal spacing of the pump interference minima, and leads to the scaling of the effective FSR [Fig. 4(b)].

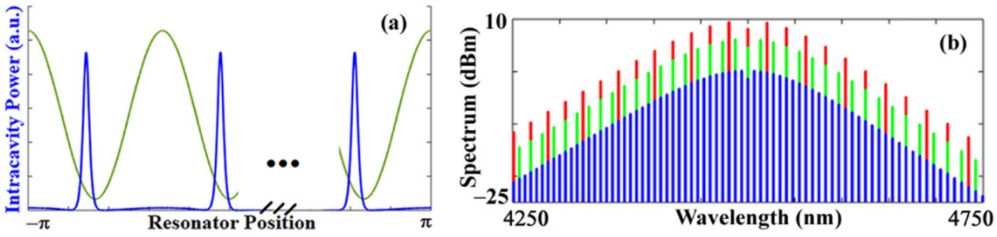

Fig. 4. (a) Schematic of multiple solitons (blue) present in a resonator with a pump wave as a function of resonator position. The preferred pulse positions are near, but do not coincide with, the minima of the pump interference pattern in green. (b) Spectra of one (blue), two (green), and three (red) equally spaced solitons. Note the increase in total power (efficiency) owing to the increase in the number of intracavity solitons.

Figure 5(a) and (b) show the evolution of two and three unevenly spaced solitons in a TOD resonator when a second pump with P_2/P_1 = 60% and δ_{12} = 2 and 3 is turned on at 150 ns for Fig. 5(a) and at 0 ns for Fig. 5(b). In response, the effective soliton velocity increases until the pulses reach the preferred locations close to the pump interference minima. Upon relaxation oscillations, the pulses remain locked in their evenly spaced positions relative to the group velocity as long as the second pump remains on.

Optics EXPRESS

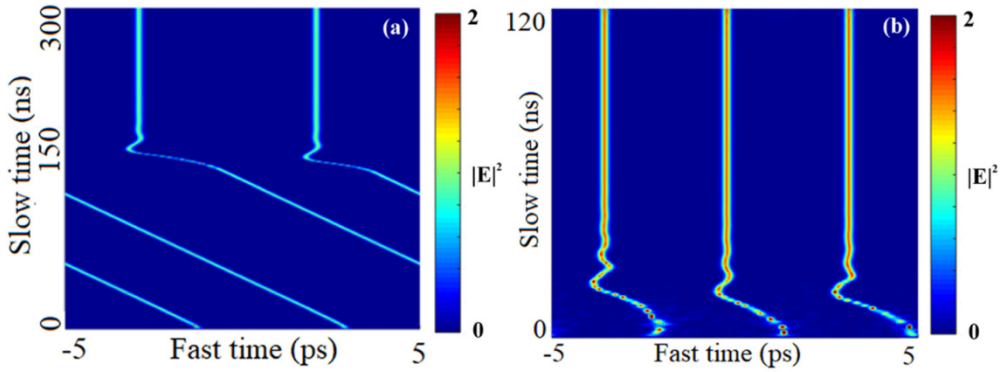

Fig. 5. (a) Two pulses locked by turning on a second pump two FSRs away (δ_{12} = 2) at 150 ns and (b) Three pulses locked into place by a second pump with δ_{12} = 3. In both cases, P_2/P_1 = 60% and Δ = 31.5.

A single soliton comb in this system has an external nonlinear conversion efficiency of η_c ≈0.77%, which increases to $2\eta_c$ and $3\eta_c$ for the two-soliton and three-soliton combs, respectively. However, statistical studies imply a practical upper limit of two on the number of solitons that can be reliably generated using bichromatic pumping in this system. This is because three or more solitons only very rarely emerge from the noise with a spacing close enough to optimal (so that they do not collide and annihilate). The practical upper limit should be lower in systems with weaker dispersion. Since these pulses are formed after the system goes through the chaotic state as the detuning is increased, these multiple-pulse solutions have a different existence range than Turing rolls.

The tendency of the pulses to rest at positions near, but not coinciding with the minima of the pump interference wave could be problematic in a system with significant pump-power fluctuations. Since only the spacing between the extrema is independent of pump power, it is desirable for the pulses to rest at the minima or maxima [12].

5. Parameter limitations on bichromatic pumping

5.1 Limitations on detuning

In this section, we investigate the effect of changing δ_{12}, P_2/P_1, and α. Figure 6(a) shows the creation of a single soliton, starting from noise, by increasing the detunings of both pumps from Δ = 0 to Δ = 31.5 over 300 ns in steps of Δ = 0.5 every 5 ns for δ_{12} = 1 and P_2/P_1 = 40%. When the pulse is created after ≈300 ns, it rotates around the simulation window, as for monochromatic pumping, but with a varying velocity that depends on the position of the pulse in the resonator. When the pulse is close to the preferred pulse position slightly to the left of the center of the resonator (τ = 0), its velocity decreases owing to an effective force exerted by the second pump. However, this force is not strong enough to counteract the tendency of the pulse to rotate relative to the group velocity induced by higher-order dispersion.

Optics EXPRESS

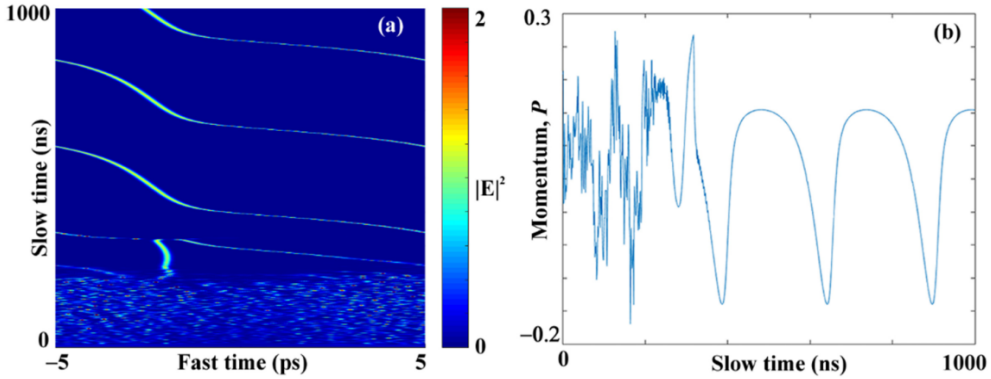

Fig. 6. (a) Generation and evolution of a single soliton in a system with $\delta_{12} = 1$ and $P_2/P_1 = 40\%$. The detunings of both pumps is increased from $\Delta = 0$ to $\Delta = 31.5$ over 300 ns in steps of $\Delta = 0.5$ every 5 ns and remains constant after 300 ns. (b) Calculated momentum corresponding to the evolution depicted in (a).

The forces involved are outlined in Fig. 6(b), which shows the calculated momentum of the intracavity field as a function of slow time. During the chaotic stage of comb formation, the momentum varies unpredictably, depending on which solitons are breathing up or down at any given time. After 300 ns, the momentum converges to a periodic pattern related to the pulse rotation around the resonator. When the pulse slows down near the preferred position, the momentum is nearly stable for a short period of time. As the pulse moves away from the preferred position, the momentum changes sign and then returns to the original value. While the momentum oscillates, the pulse velocity increases as it rotates back to its preferred position.

In this case, the second pump is too weak to stabilize the pulse position. The stabilization of the pulse position and hence the repetition rate can be achieved by either boosting P_2/P_1 or decreasing the detuning. Both of these actions have a similar effect in that more of the second pump power is coupled into the resonator.

Figure 7 shows the effect of decreasing the detuning in a system with $\delta_{12} = 1$ and $P_2/P_1 = 40\%$. A single soliton rotates around the simulation window as before, at a slower rate on the left side of the pump minimum and faster to the right. At 250 ns, the pump detuning on both pumps is decreased from $\Delta = 31.5$ to $\Delta = 25$. The pulse then stabilizes its position in the resonator relative to the group velocity. We will show below that this mechanism operates only for a limited range of P_2/P_1. The opposite effect can be observed by starting with a stabilized pulse in Fig. 8 with $\delta_{12} = 1$ and $P_2/P_1 = 60\%$ and increasing the detuning from $\Delta = 31.5$ to $\Delta = 60$ (in discrete steps of $\Delta = 0.5$ every 10 ns, starting from $t = 0$ and ending at $t = 570$ ns). Since less power is coupled in at larger detunings because we are on the effectively red detuned side of the bistable resonance, the pulse shifts initially to the left, closer to its new preferred position, but after a few hundred ns becomes destabilized.

Optics EXPRESS

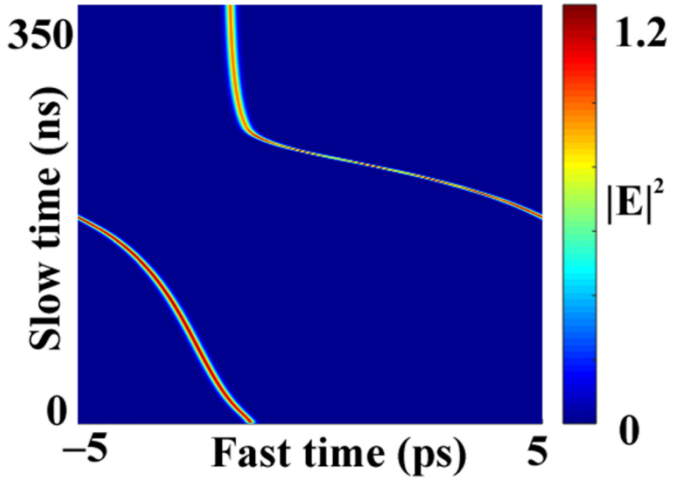

Fig. 7. A single soliton in a system with $\delta_{12} = 1$ and $P_2/P_1 = 40\%$, stabilized by instantaneously decreasing the pump detuning from $\Delta = 31.5$ to $\Delta = 25$ at 250 ns.

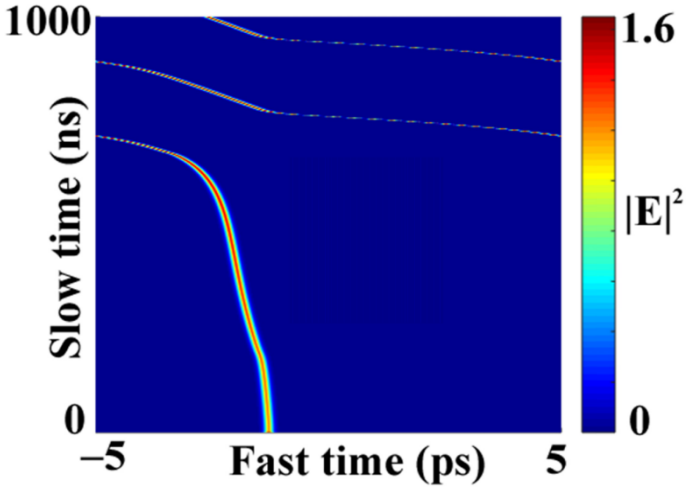

Fig. 8. A soliton in a system with $\delta_{12} = 1$ and $P_2/P_1 = 60\%$ as the detuning is increased from $\Delta = 31.5$ by 0.5 every 10 ns, starting from $t = 0$ and ending at $t = 570$ ns. The pulse, whose position is initially unstable, begins to rotate around the simulation window.

If the detuning is decreased for fixed pump powers, the position of the pulse shifts closer to the minimum at $\tau = 0$ until the detuning is so small that the resonator reverts to the chaotic state (see Appendix A).

The optimal detuning for bichromatic pumping is smaller (larger) when the total pump power is lower (higher), as in the monochromatic case. Figure 9 shows two cases for a system with TOD and $P_2/P_1 = 60\%$ when P_1 is halved to 2.5 mW. The pulse position is stabilized when $\Delta = 20$ [Fig. 9(b)], but not when $\Delta = 31.5$ [Fig. 9(a)].

Optics EXPRESS

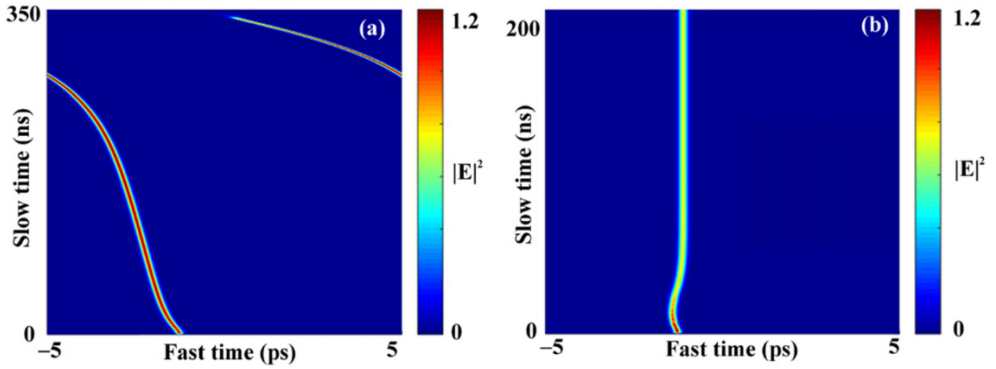

Fig. 9. A system with TOD and P_2/P_1 = 60% and P_1 = 2.5 mW (a) Δ = 31.5, (b) Δ = 20.

The two pumps need not have exactly the same detuning to stabilize the soliton position. As shown in Appendix A, for P_2/P_1 = 60%, similar steady-steady solutions with a slight shift of the soliton position in the resonator are obtained when the two detunings have significantly different values. However, for effective stabilization of the repetition rate, both detunings should be in the range in which a single stable soliton exists.

5.2 Limitations onrelative second pump power

Section 5.1 showed that when P_2/P_1 or P_1 is decreased, the detuning must also be reduced in order to maintain stabilization of the repetition rate. However, when $P_2/P_1 \lesssim r_{cr}$, a decrease in the detuning will never result in a stable pulse position or repetition rate. The exact value of r_{cr} scales with the magnitude of the higher-order dispersion terms.

On the other hand, as P_2/P_1 increases well above r_{cr}, the detuning range needed to obtain a stable pulse position is wider. Figures 10(a)–10(d) show the pulse evolution in systems with TOD and P_2/P_1 = 70, 80, 90, and 95%. The stable pulse position shifts toward the minimum at τ = 0 as P_2/P_1 increases because the modulation depth of the pump interference pattern is now larger. The pulse also moves to its stable position more quickly, which results in overshoot and oscillation in Figs. 10(c) and 10(d). However, when $P_2/P_1 \approx 1$, the pulse is so close to the null that the pump power it experiences is too low to support it. This effect defines the full range for the existence of stable solitons: $r_{cr} \lesssim P_2/P_1 \lesssim R_{cr}$, with $R_{cr} \approx 97\%$, as determined in Appendix A.

Optics EXPRESS

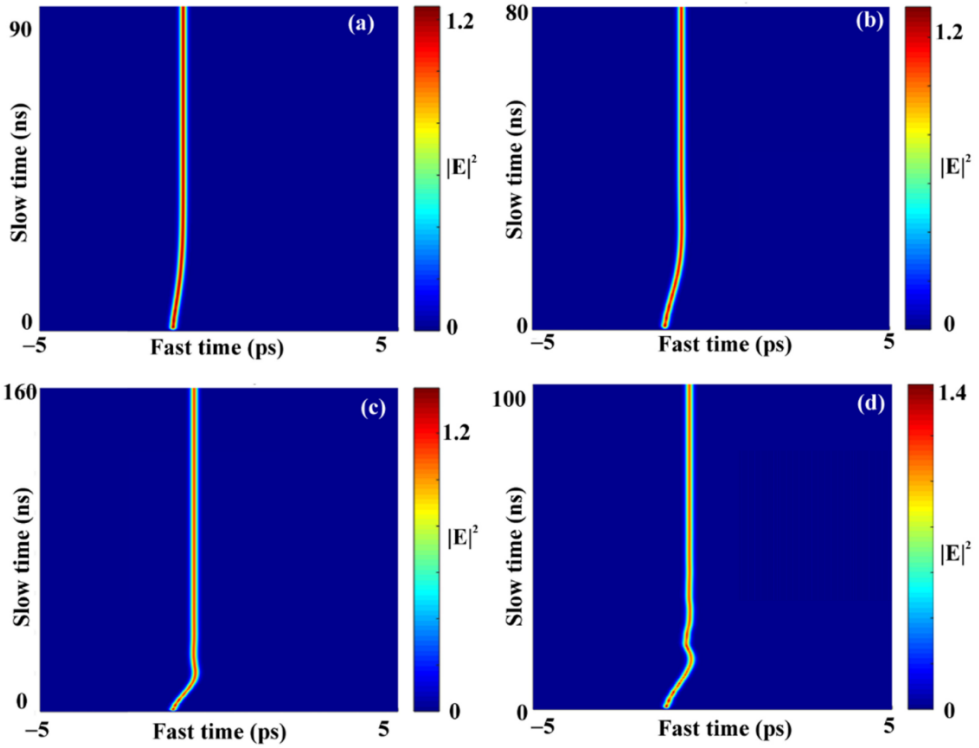

Fig. 10. Evolution of the P_2/P_1 = 60% TOD steady-state solution for systems with (a) P_2/P_1 = 70%, (b) P_2/P_1 = 80%, (c) P_2/P_1 = 90%, (d) P_2/P_1 = 95%. For all cases, the detuning is Δ = 31.5.

Similarly, there are upper and lower limits of the detuning that depend on P_2/P_1. These limits are considered in more detail in Section 6.

5.3 Limitations on loss

When the pulse is close to the pump interference wave null, the pump power the pulse experiences is reduced. If the loss is high enough, the pump power becomes insufficient to support the existence of a pulse. Even if the loss is below that limit, the total effective bichromatic pump power seen by the pulse may be too low to stabilize its position. We investigate this effect by seeding the TOD simulations with stabilized pulses at a particular value of P_2/P_1, and then simultaneously increasing the material loss, α_i, and the main pump power, P_1, by a small amount while keeping P_2/P_1, θ/α_i, and δ_0 constant. Figure 11 shows the limiting values of the power coupling coefficient, 2α, and the corresponding Q factors for which the pulse position is no longer stabilized and for which the pulse no longer exists as a function of P_2/P_1. While these boundaries depend on the exact detuning and pump power, Fig. 11 demonstrates that the upper limit on the loss for stabilized pulses is quite low for this particular system. If the higher-order dispersion terms are smaller, the "force" on the pulse does not need to be nearly as strong to counteract the dispersion, and the stabilization limit is significantly relaxed.

Optics EXPRESS

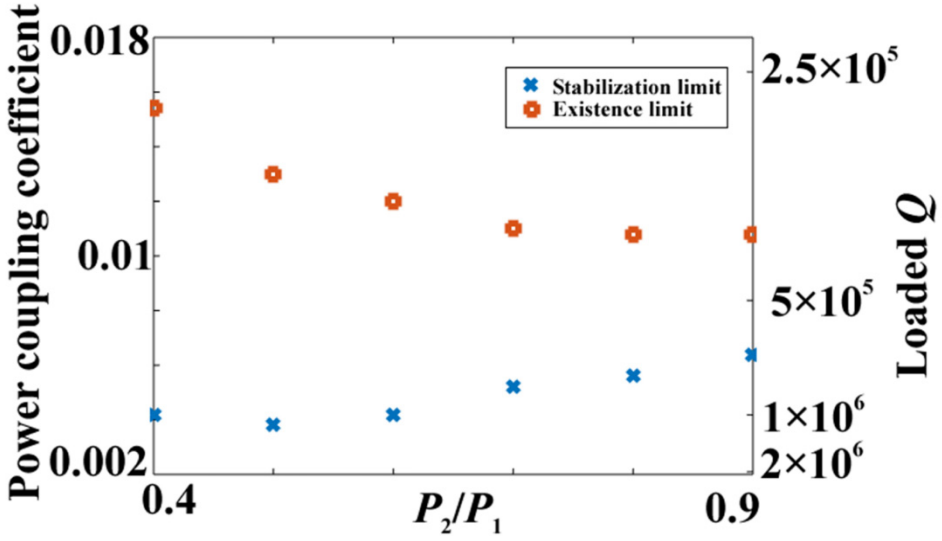

Fig. 11. Boundaries above which the pulse is no longer in a stable position (blue) or supported (orange) due to insufficient pump power, for values of P_2/P_1 where stabilized pulses exist with TOD. The detuning for the stabilized pulses is $\delta_0 = 0.04725$ for all points except $P_2/P_1 = 0.4$, which uses $\delta_0 = 0.0386$. The main pump power, P_1, scales linearly with α, starting at $P_1 = 5$ mW for $\alpha = 0.0016$.

5.4 Second pump on long wavelength side

Figure 12 shows the generation of a single soliton starting from noise in a system with TOD, $\delta_{12} = -1$, and $P_2/P_1 = 60\%$. A single soliton is again generated in a stable position, but on the opposite side of the pump wave interference minimum.

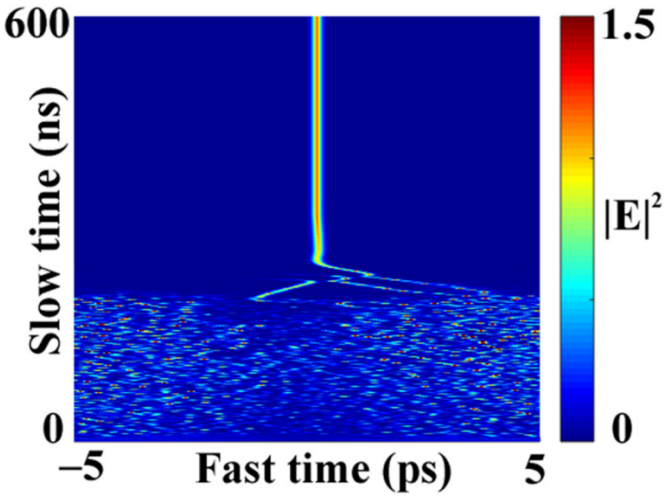

Fig. 12. A single, stabilized soliton generated from noise by increasing the detuning from $\Delta = 0$ to $\Delta = 31.5$, in a system with TOD, $\delta_{12} = -1$ and $P_2/P_1 = 60\%$.

Even though the intracavity power fields are identical apart from the shift in resonator position when $\delta_{12} = 1$ or $\delta_{12} = -1$, the real and imaginary parts that make up the intracavity scalar field E are different. Therefore, the momentum calculated from Eq. (2) also differs when $\delta_{12} < 0$, which explains the change in the stable pulse position in each case. Figure 13 shows the real parts of the electric-field profile in the resonator for $\delta_{12} = 1$ and $\delta_{12} = -1$ with

Optics EXPRESS

P_2/P_1 = 60%. While the specific stabilized position in the resonator is of little practical importance in and of itself, its proximity to the pump minimum leads to a shift of the parameter boundaries. In particular, R_{cr} becomes significantly smaller because the stabile position is closer to the intracavity pump minimum for $\delta_{12} = -1$. This effect is illustrated in the examples given in Appendix A.

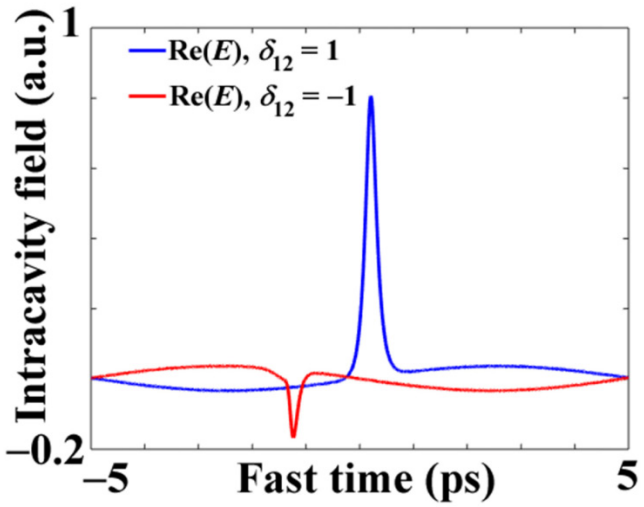

Fig. 13. Real components of the intracavity field profile for a TOD system with bichromatic pumping with P_2/P_1 = 60% and δ_{12} = 1 (red) and δ_{12} = −1 (blue).

5.5 Results with two sidebands

In some experimental scenarios, e.g. when the amplitude of the pump is modulated at a sufficiently high frequency, two secondary pumps, on both sides of the main pump, are introduced into the cavity (δ_{12} = 1 and δ_{13} = −1). Figure 14(a) shows that the pulse position can be stabilized under these conditions with weaker relative powers $P_2/P_1 = P_3/P_1$ = 20%. In this simulation, the normalized detuning is increased by Δ = 1 every 10 ns, up to a maximum of Δ = 25, at which the pulse position becomes stable from about 300 to 350 ns. In Fig. 14(a), the normalized detuning at 380 ns is abruptly increased to Δ = 28, and the pulse velocity increases, as expected from earlier results. With two sidebands, the modulation depth of the overall pump profile is greater, and the minimum pump power near the stable pulse position is lower. To keep the pulse stable, either the detuning must be decreased or P_2/P_1 and P_3/P_1 must be higher. The latter case with $P_2/P_1 = P_3/P_1$ = 50% is shown in Fig. 14(b), in which the pulse position is stable in this system with Δ = 28.

Optics EXPRESS

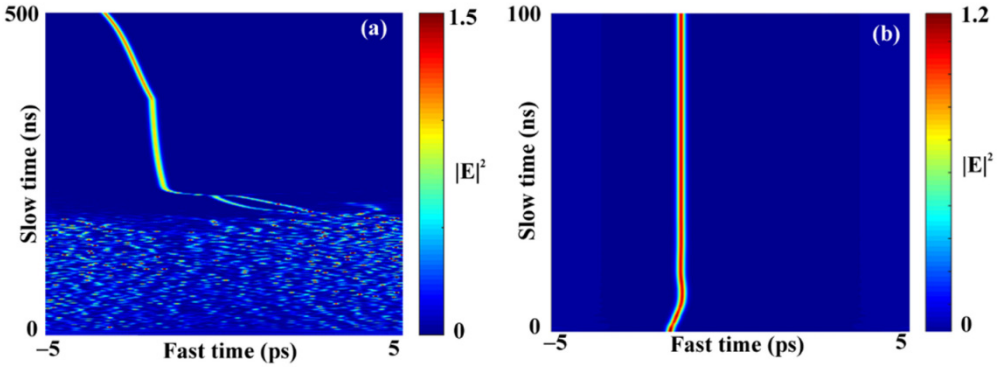

Fig. 14. (a) Single pulse generation and evolution in a TOD system with high- and low-frequency secondary pumps with $P_2/P_1 = P_3/P_1 = 20\%$. In (a), initially the normalized detuning is increased by $\Delta = 1$ every 10 ns, up to a maximum of $\Delta = 25$. The detuning is instantaneously increased to $\Delta = 28$ at 380 ns, which delocalizes the pulse. (b) The steady-state solution from (a) in a TOD system with high- and low-frequency secondary pumps with $P_2/P_1 = P_3/P_1 = 50\%$ and $\Delta = 28$.

6. Relative power and detuning boundaries

Motivated by the results of Section 5, we proceed to determine the full range of detuning and relative pump powers that yield stabilized pulse positions and hence a stabilized repetition rate. To that end, Figs. 15 and 16 show the approximate stability boundaries for systems with TOD and 6OD. These are obtained by first stabilizing a pulse at some P_2/P_1 and a detuning $\Delta \approx 30$, and then increasing the detuning slowly to $\Delta_{max}(P_2/P_1)$ for Region I until the pulse location is no longer stable. To determine $\Delta_{min}(P_2/P_1)$ for Region I, P_2/P_1 is kept fixed, while the detuning is reduced until the pulse transitions into the low-power CW branch solution or a chaotic multipulse state. Not shown in Figs. 15 and 16 is the absolute upper bound of stable solitons, at which point the system goes over to the low-power CW solution. That boundary is quite analogous to the case of monochromatic pumping with detuning that is too high [5,22]. The results in Figs. 15 and 16 provide an outline of the regions of repetition rate stability whose boundaries can be pinpointed with greater accuracy using linearized stability analysis [23,24]. The boundaries in Figs. 15 and 16 are approximate due to the ambiguity of pulse stability in an evolutionary method. For example, a pulse that appears stabilized may in fact be moving very slowly. The linearized stability analysis for this system will be discussed in a future work.

Optics EXPRESS

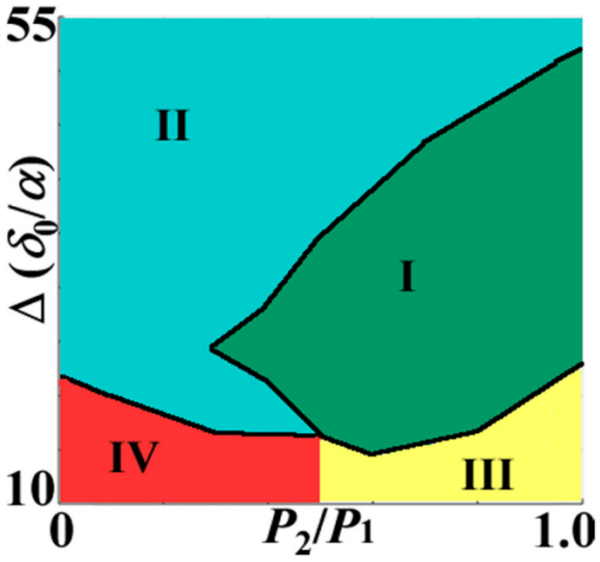

Fig. 15. Stability boundaries for TOD and δ_{12} = 1: in Region I the pulse position is stable, in Region II the pulse rotates because the detuning is too high, in Region III the single pulse solution goes back to a chaotic multipulse state, and in Region IV the pulse disappears, and the system transitions to a low-power CW solution.

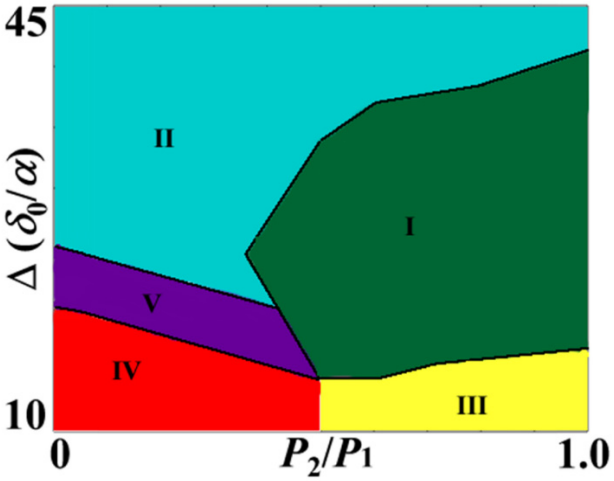

Fig. 16. Stability boundaries for 6OD and δ_{12} = 1. The meanings of Regions I-IV are the same as in Fig. 15, while in Region V the pulse breathes in amplitude and width as it rotates.

Figures 15 and 16 show that the stability boundaries are broadly the same for systems with TOD and 6OD. The same is true of all-order dispersion, which implies convergence to a qualitatively similar picture of the different regions. However, the comb spectra do show pronounced differences between TOD and 6OD, owing to the presence of a second, long-wavelength dispersive wave in the 6OD (and AOD) case. Additionally, Region V is not present with only TOD because of the increase in complexity of the soliton dynamics with 6OD due to the presence of the long-wavelength dispersive wave. The statistics of the pulse generation are also different in each case, as discussed in Section 8. However, the qualitative similarity in the stability regions even when the comb spectra are significantly qualitatively and quantitatively different indicates that similar boundaries may exist in general for many different systems with higher-order dispersion.

Optics EXPRESS

7. Comparison to second-order dispersion

When only second-order dispersion is present, the solitons generated by monochromatic pumping are generally stationary relative to the group velocity (see Appendix B). With a second pump, the behavior is similar to the case of higher-order dispersion, as shown in Fig. 17. Here two pulses are generated and forced to the same resonator position, where they collide, which causes the annihilation of one of the pulses, while the other survives. Of course, in this case, the second pump is not needed to stabilize the soliton position, since it is stable under monochromatic pumping. In other words, there is no lower bound on P_2/P_1. However, the influence of the second pump that pushes generated solitons to the same location increases the likelihood that only a single soliton survives compared to the monochromatic case.

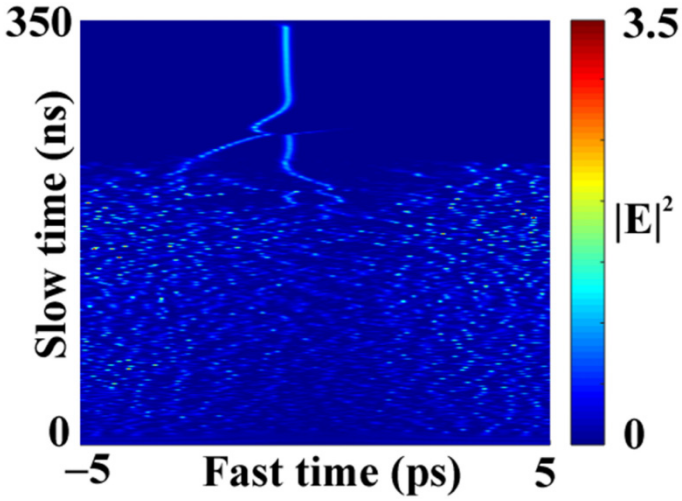

Fig. 17. Single pulse generation and evolution in a system with SOD and bichromatic pumping with $P_2/P_1 = 60\%$, $\Delta = 31.5$, and $\delta_{12} = 1$.

A few other notable differences with the higher-dispersion scenarios are found to exist: (1) pulses created on the left side of the resonator minimum cannot cross the center when $P_2/P_1 \lesssim 70\%$; and (2) the upper limit on P_2/P_1 is much lower, as illustrated in Appendix B.

8. Statistics of pulse generation

We have also investigated the statistical properties of soliton generation with bichromatic pumping, i.e., how likely it is that a soliton is generated starting from noise. Figure 18 shows a histogram for the number of solitons created in the system with TOD over $N = 1100$ runs with $\delta_{12} = 1$ and $P_2/P_1 = 60\%$. A single soliton is generated in nearly exactly one half of the runs. When no solitons are generated after the system stabilizes, the resonator may initially contain an even number of solitons that annihilate pairwise in collisions that occur as they move toward the preferred position in the resonator. This scenario is illustrated in Fig. 19.

Optics EXPRESS

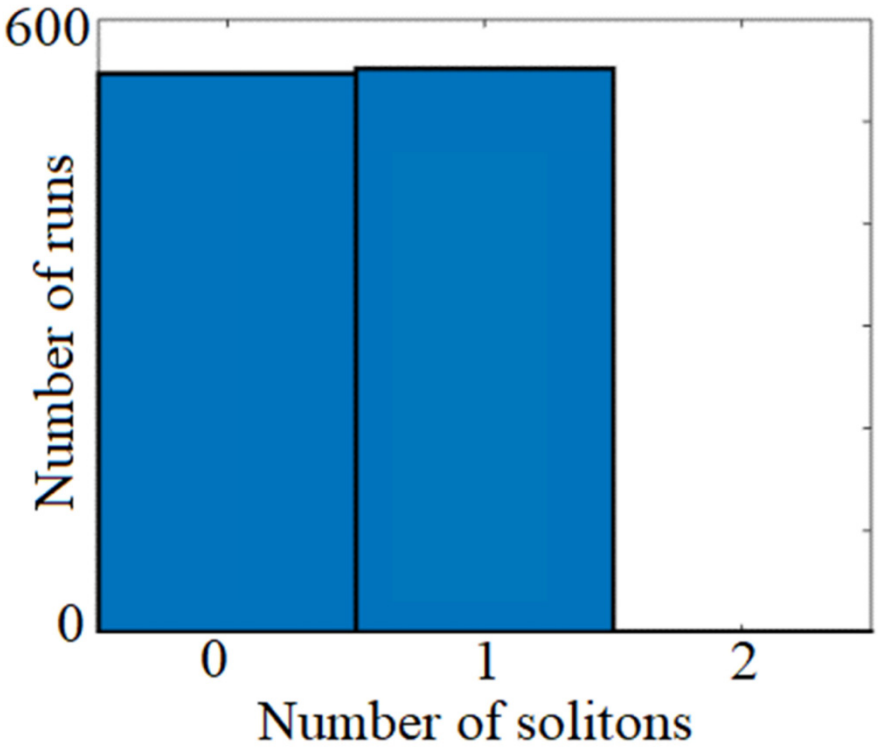

Fig. 18. Histogram of the number of pulses created in simulations of a system with TOD, δ_{12} = 1, and P_2/P_1 = 60% over 1100 runs. $N(0)$ = 548, $N(1)$ = 552. Simulations are carried out from noise by increasing the detuning as shown by Fig. 19.

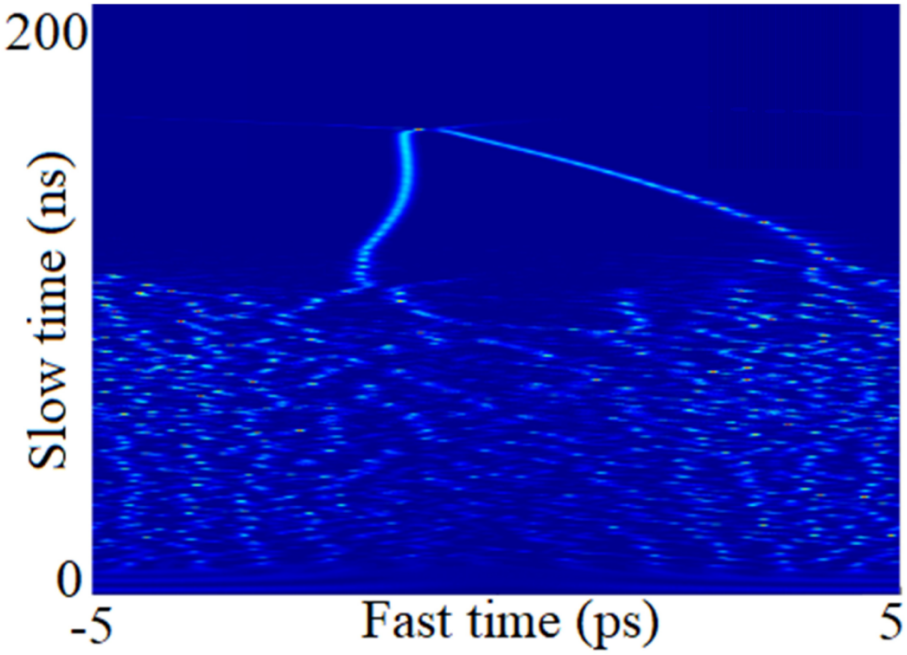

Fig. 19. Generation and annihilation of two solitons in a system with TOD, P_2/P_1 = 60%, and δ_{12} = 1. Detuning increases from $\Delta = 0$ to $\Delta = 30$ at a rate of 1 every 5 ns.

Optics EXPRESS

The statistics of the soliton generation vary depending on the dispersion order. For example, in a system with 6OD and bichromatic pumping, the ratio of single-soliton cases to zero-soliton cases is much lower: $N(1)/N(0) \approx 0.2$, but for AOD, it increases to $N(1)/N(0) \approx 0.5$. The statistics are more favorable for AOD than 6OD because the long-wavelength dispersive wave is red-shifted for AOD compared to 6OD, so that high-frequency interference between the two dispersive waves is reduced. In spite of these apparent statistical differences, the regime boundaries given in Fig. 16 remain nearly identical for the cases of 6OD and AOD.

9. Conclusion

We have investigated bichromatic pumping of microresonator frequency combs with higher-order dispersion. The potential pumps that satisfy the requirements include a monolithic two-color pump, two distinct lasers with closely spaced lines, or a pump that is strongly amplitude modulated at the FSR frequency to create two symmetric subbands. We showed that such pumping of a microresonator with arbitrary dispersion can be a viable route to a stable frequency comb with a fixed repetition rate, provided that the relative power at each pump frequency and the frequency difference remain within the limits that the simulations show to be favorable. This work confirms that dual pumping can be used in systems with higher-order dispersion to stabilize the pulse position and the repetition rate of the comb.

The stability region exhibits an upper limit due to the relative strength of the second pump that arises because the standing-wave pattern in the resonator lowers the pump intensity near the preferred operating position of the pulse. The upper limit of P_2/P_1 is nearly independent of the truncation of the dispersion orders in the simulation beyond the second order. A lower limit on P_2/P_1 also exists for systems with dispersion orders higher than second, and is estimated to be between $P_2/P_1 \approx 40\%$ to 60%, depending how many dispersion orders are included and how large they are. There is no practical lower limit on the relative pump powers if the dispersion orders beyond the second are negligible, but the stabilization time increases significantly as the relative strength of the second pump is decreased. Because the preferred operating position of the pulse is close to the pump wave minimum, the stabilization effect is sensitive to the total loss. If the loss exceeds a few tenths of a percent per round trip (with cavity Q in the 10^5 range), the repetition rate stabilization effect becomes impossible to realize. Future work will increase the accuracy of the stability boundaries outlined in this work by using a linearized stability analysis of the LLE with bichromatic pumping.

Multiple solitons can be stabilized in the resonator if the two pumps are separated by multiples of the FSR with similar (but not necessarily exactly the same) detuning from the nearest resonator mode. The practical advantage of this configuration is that the conversion efficiency scales with the number of the solitons in the resonator. In practice, the number of solitons that can be stabilized in an appreciable fraction of the runs depends on the magnitude of the higher-order dispersion terms, even though the boundaries of the stable region are only weakly affected by the inclusion of terms higher than the third.

Taheri et al. [6] showed that the repetition rate is sensitive to the difference in the actual pump frequencies, which may lead to variations in the repetition rate in a bichromatically pumped system. This is particularly true for independent pump sources, where the frequency noise is not highly correlated. However, this problem may be mitigated by a specially designed dual-wavelength distributed-feedback emitter, which could be integrated on the same chip as the microresonator.

During the review, the authors were alerted to an advance publication on microresonator-based dual-pump optical memory buffers that also includes third-order dispersion [25].

Appendix A: Additional TOD results

The opposite of the dynamics in Fig. 8, which shows results for increasing detuning, occurs when the detuning is decreased. This scenario is illustrated in Fig. 20 (a) and (b), which show a system with TOD and $P_2/P_1 = 60\%$ as the detuning is decreased from $\Delta = 31.5$ to $\Delta = 21.5$

Optics EXPRESS

in Fig. 20(a) and further from Δ = 21.5 to Δ = 14.5 in Fig. 20(b), both at a rate of Δ = 0.1 per 10 ns. The effect of decreasing the detuning in a stabilized system is simply to shift the preferred pulse position closer to the resonator minimum at $\tau = 0$. However, if the detuning becomes sufficiently small, the soliton is no longer stable, and the system reverts to a chaotic state characteristic of lower detuning. This chaotic state is visible at the top of Fig. 20(b) as bright spots that indicate the presence of other solitons produced by the CW tails of the formerly stable single soliton. The amplitude of the tail can also be seen increasing as the detuning is decreased.

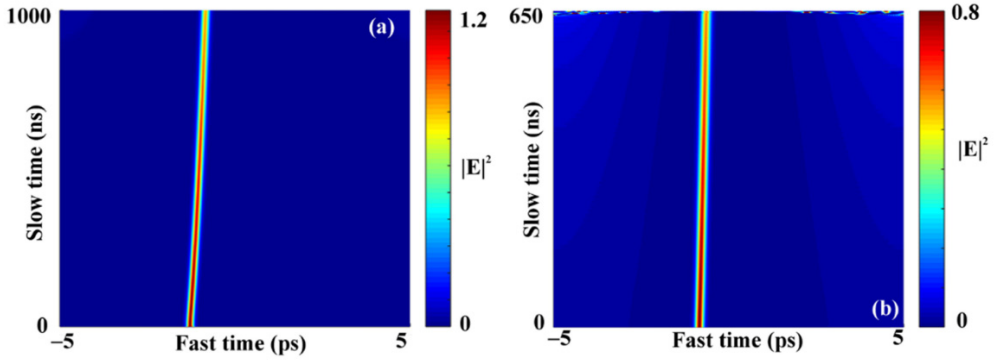

Fig. 20. Decreasing the detuning in a stabilized system with a single soliton with TOD, P_2/P_1 = 60%, and $\delta_{12} = 1$. (a) The detuning is decreased from Δ = 30 to 21.5. (b) The detuning is decreased further from Δ = 21.5 to 14.5.

Figure 21 shows the effect of different detuning for the two pumps. The P_2/P_1 = 60% TOD steady-state solution obtained for Δ = 31.5 for both pumps is an initial condition to a system in which only the detuning of the second pump is changed to Δ = 25.5. After moving left in the resonator, the pulse position is once again stable. This result shows that the two pumps need not have exactly the same detuning to achieve the repetition rate stabilization effect.

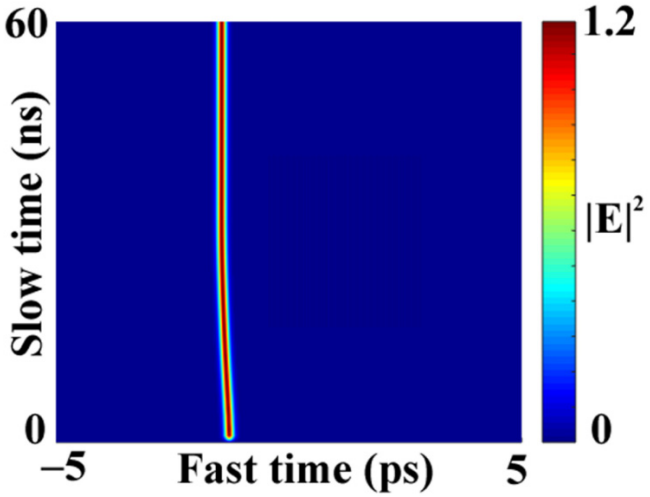

Fig. 21. Pulse evolution with main pump detuning Δ_1 = 31.5 and second pump detuning Δ_2 = 25.5 with $\delta_{12} = 1$.

Optics EXPRESS

When $P_2 \approx P_1$, the pulse moves so close to the pump null that it cannot survive because the pump power at that position is too low to sustain the pulse, as shown in Fig. 22. The exact boundary depends on the exact initial conditions, but the general upper limit is $P_2/P_1 \approx 97\%$.

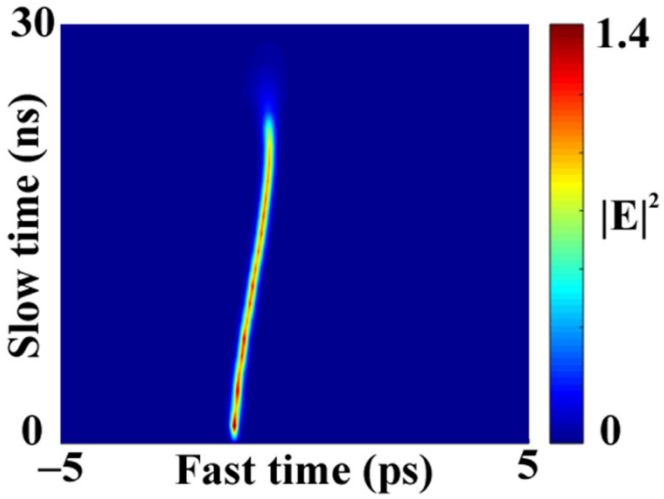

Fig. 22. Evolution of the $P_2/P_1 = 60\%$ TOD $\delta_{12} = 1$ steady-state solution for a system with $P_2/P_1 = 98\%$.

When the second pump is on the low-frequency side of the main pump ($\delta_{12} < 0$), the parameter boundaries for stable pulses are different from the $\delta_{12} > 0$ case. This is illustrated in Fig. 23, which shows the steady-state pulse solution from Fig. 12, with the initial position of the pulse shifted to the right by one quarter of the resonator circumference, in a TOD system with $P_2/P_1 = 70\%$ and $\delta_{12} = -1$. In this pumping scenario, the pulse quickly disappears. (The same behavior is observed when the pulse is not shifted.)

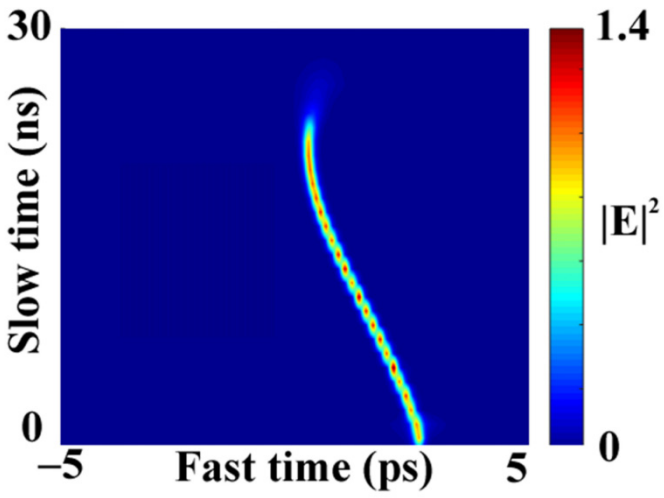

Fig. 23. Pulse evolution for the shifted steady-state solution from Fig. 12 in a system with TOD, $\delta_{12} = -1$, and $P_2/P_1 = 70\%$.

Appendix B: Additional SOD results

When only second-order dispersion is present in the system, solitons propagate at the group velocity, as illustrated for a monochromatic pump in Fig. 24. Initially, three pulses are

Optics EXPRESS

generated, and their position is fixed until all but one disappear at higher detuning. The position of the surviving pulse is also fixed. The positions of the pulses are modified only by soliton collisions, which are visible just after pulses emerge from the chaotic state.

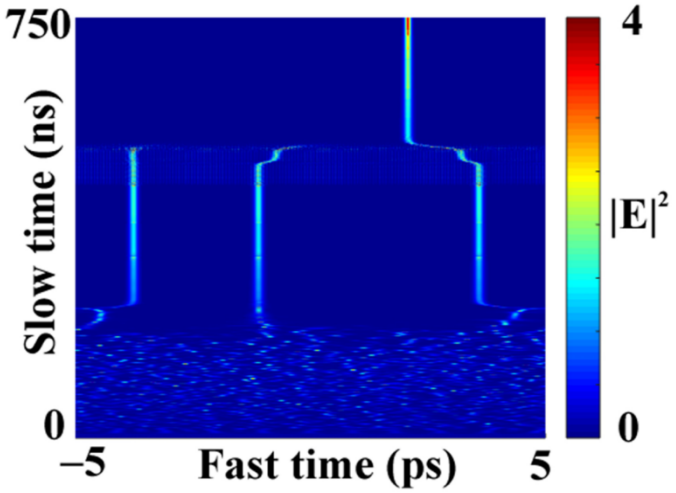

Fig. 24. Soliton creation and evolution in a system with SOD and monochromatic pumping. The detuning is increased from $\Delta = 0$ to $\Delta = 75$ at a rate of 0.5 per 5 ns.

There is no lower limit to the relative pump power for pulse stabilization in the SOD case, because the pulse position is fixed even under monochromatic pumping. Under bichromatic pumping with a weak second pump, a generated soliton will move to the stable position shown in Fig. 17, but at a slower rate as the second pump power is decreased.

Figure 25 shows the evolution of the steady-state pulse in SOD systems with $P_2/P_1 = 86\%$ for Fig. 25(a) and 87% for Fig. 25 (b), which indicates that $86\% < R_{cr} < 87\%$, i.e., significantly lower than in the TOD case. R_{cr} may be even lower if the pulse is not generated near the stable position, as shown in Fig. 26 for a system with SOD and $P_2/P_1 = 70\%$.

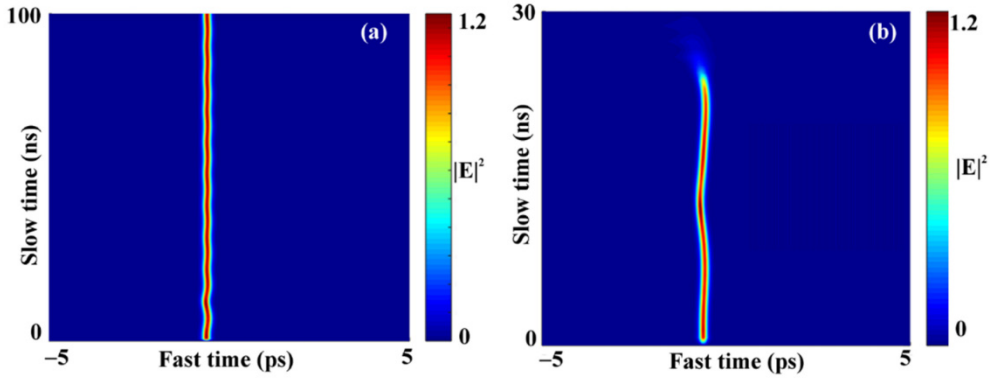

Fig. 25. (a) Evolution of the steady-state solution from Fig. 16 in a SOD system with $P_2/P_1 = 86\%$ and $\delta_{12} = 1$. (b) Evolution of the steady-state solution from Fig. 16 in a SOD system with $P_2/P_1 = 87\%$ and $\delta_{12} = 1$.

Optics EXPRESS

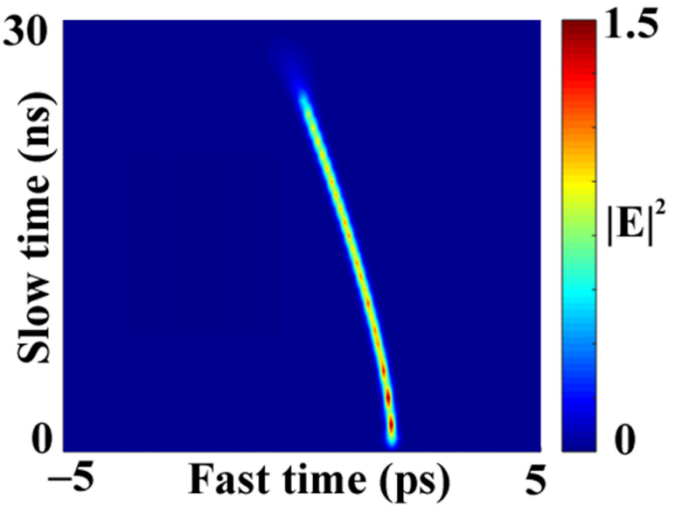

Fig. 26. Evolution of the shifted steady-state solution from Fig. B1 in a SOD system with P_2/P_1 = 70% and δ_{12} = 1.

References

1. A. Schliesser, N. Picqué, and T. W. Hänsch, "Mid-infrared frequency combs," Nat. Photonics **6**(7), 440–449 (2012).
2. M. Pu, L. Ottaviano, E. Semenova, and K. Yvind, "Efficient frequency comb generation in AlGaAs-on-insulator," Optica **3**(8), 823–826 (2016).
3. M. Sheik-Bahae, D. C. Hutchings, D. J. Hagan, and E. W. Van Stryland, "Dispersion of bound electron nonlinear refraction in solids," IEEE J. Quantum Electron. **27**(6), 1296–1309 (1991).
4. M. Yu, Y. Okawachi, A. G. Griffith, N. Picqué, M. Lipson, and A. L. Gaeta, "Silicon-chip-based mid-infrared dual-comb spectroscopy," Nat. Commun. **9**(1), 1869 (2018).
5. C. Bao, H. Taheri, L. Zhang, A. Matsko, Y. Yan, P. Liao, L. Maleki, and A. E. Willner, "High-order dispersion in Kerr comb oscillators," J. Opt. Soc. Am. B **34**(4), 715–725 (2017).
6. H. Taheri, A. B. Matsko, and L. Maleki, "Optical Lattice Trap for Kerr Solitons," Eur. Phys. J. D **71**(6), 153 (2017).
7. D. V. Strekalov and N. Yu, "Generation of optical combs in a whispering gallery mode resonator from a bichromatic pump," Phys. Rev. A **79**(4), 41805 (2009).
8. V. E. Lobanov, G. V. Lihachev, N. G. Pavlov, A. V. Cherenkov, T. J. Kippenberg, and M. L. Gorodetsky, "Harmonization of chaos into a soliton in Kerr frequency combs," Opt. Express **24**(24), 27382–27394 (2016).
9. T. Hansson and S. Wabnitz, "Bichromatically pumped microresonator frequency combs," Phys. Rev. A **90**(1), 013811 (2014).
10. H. Taheri, A. A. Eftekhar, K. Wiesenfeld, and A. Adibi, "Soliton formation in whispering-gallery-mode resonators via input phase modulation," IEEE Photonics J. **7**(2), 1–9 (2015).
11. S. B. Papp, P. Del'Haye, and S. A. Diddams, "Parametric seeding of a microresonator optical frequency comb," Opt. Express **21**(15), 17615–17624 (2013).
12. are I. Hendry, W. Chen, Y. Wang, B. Garbin, J. Javaloyes, G.-L. Oppo, S. Coen, S. G. Murdoch, and M. Erkintalo, "Spontaneous symmetry breaking and trapping of temporal Kerr cavity solitons by pulsed or amplitude-modulated driving fields," Phys. Rev. A (Coll. Park) **97**(5), 053834 (2018).
13. C. Bao, L. Zhang, A. Matsko, Y. Yan, Z. Zhao, G. Xie, A. M. Agarwal, L. C. Kimerling, J. Michel, L. Maleki, and A. E. Willner, "Nonlinear conversion efficiency in Kerr frequency comb generation," Opt. Lett. **39**(21), 6126–6129 (2014).
14. Y. K. Chembo and C. R. Menyuk, "Spatiotemporal Lugiato-Lefever formalism for Kerr-comb generation in whispering-gallery-mode resonators," Phys. Rev. A **87**(5), 053852 (2013).
15. M. Erkintalo and S. Coen, "Coherence properties of Kerr frequency combs," Opt. Lett. **39**(2), 283–286 (2014).
16. J. U. Kang, A. Villeneuve, M. Sheik-Bahae, G. I. Stegeman, K. Al-hemyari, J. S. Aitchison, and C. N. Ironside, "Limitation due to three-photon absorption on the useful spectral range for nonlinear optics in AlGaAs below half band gap," Appl. Phys. Lett. **65**(2), 147–149 (1994).
17. J. M. Dudley, G. Genty, and S. Coen, "Supercontinuum generation in photonic crystal fiber," Rev. Mod. Phys. **78**(4), 1135–1184 (2006).
18. T. Jahnke, M. Mikl, and R. Schnaubelt, "Strang splitting for a semilinear Schrodinger eqaution with damping and forcing," J. Math. Anal. Appl. **455**(2), 1051–1071 (2017).

Optics EXPRESS

19. M. Yu, J. K. Jang, Y. Okawachi, A. G. Griffith, K. Luke, S. A. Miller, X. Ji, M. Lipson, and A. L. Gaeta, "Breather soliton dynamics in microresonators," Nat. Commun. **8**, 14569 (2017).
20. G. P. Agrawal, *Nonlinear Fiber Optics*, 3rd ed. (Academic, 2001).
21. E. V. Zemlyanaya and I. V. Barashenkov, "Traveling solitons in the damped-driven nonlinear schrodinger equation," SIAM J. Appl. Math. **64**(3), 800–818 (2004).
22. M. R. E. Lamont, Y. Okawachi, and A. L. Gaeta, "Route to stabilized ultrabroadband microresonator-based frequency combs," Opt. Lett. **38**(18), 3478–3481 (2013).
23. C. Godey, I. V. Balakireva, A. Coillet, and Y. K. Chembo, "Stability analysis of the spatiotemporal Lugiato-Lefever model for Kerr optical frequency combs in the anomalous and normal dispersion regimes," Phys. Rev. A **89**(6), 063814 (2014).
24. S. Wang, A. Docherty, B. S. Marks, and C. R. Menyuk, "Boundary tracking algorithms for determining the stability of mode-locked pulses," J. Opt. Soc. Am. B **31**(11), 2914–2930 (2014).
25. A. Roy, R. Haldar, and S. K. Varshney, "Robust, Synchronous Optical Buffer and Logic Operation in Dual-pump Kerr Micro-Resonator," J. Lit. Technol. **36**(24), 5807–5814 (2018), doi:10.1109/JLT.2018.2878573.